On the vortex dynamics of flow past a sphere at Re = 3700 in a uniformly stratified fluid

Karu Chongsiripinyo, Anikesh Pal, and Sutanu Sarkar

Citation: Phys. Fluids **29**, 020704 (2017); doi: 10.1063/1.4974503
View online: http://dx.doi.org/10.1063/1.4974503
View Table of Contents: http://aip.scitation.org/toc/phf/29/2
Published by the American Institute of Physics

Articles you may be interested in

Evidence of a forward energy cascade and Kolmogorov self-similarity in submesoscale ocean surface drifter observations
Phys. Fluids **29**, 020701020701 (2017); 10.1063/1.4974331

Role of head of turbulent 3-D density currents in mixing during slumping regime
Phys. Fluids **29**, 020703020703 (2017); 10.1063/1.4974353

Aerodynamics of two-dimensional flapping wings in tandem configuration
Phys. Fluids **28**, 121901121901 (2016); 10.1063/1.4971859

Modulating flow and aerodynamic characteristics of a square cylinder in crossflow using a rear jet injection
Phys. Fluids **29**, 015103015103 (2017); 10.1063/1.4972982

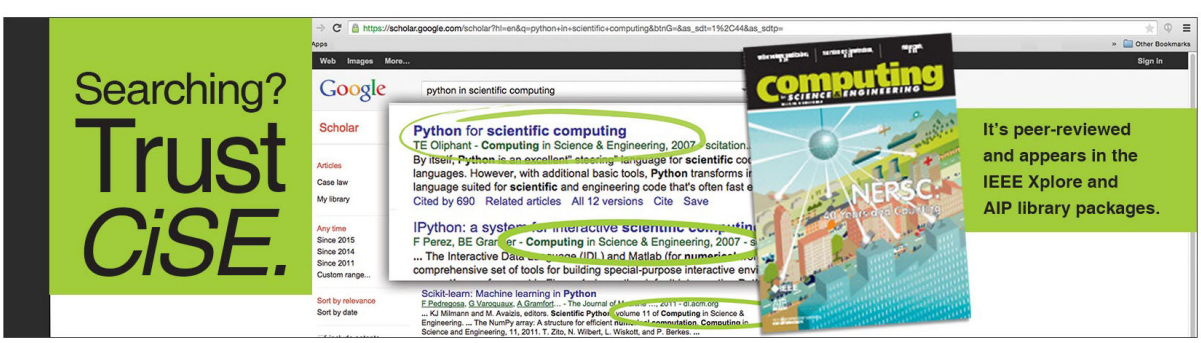

RIGHTSLINK

On the vortex dynamics of flow past a sphere at Re = 3700 in a uniformly stratified fluid

Karu Chongsiripinyo,[a] Anikesh Pal, and Sutanu Sarkar[b]
Department of Mechanical and Aerospace Engineering, University of California San Diego, San Diego, California 92093, USA

(Received 4 July 2016; accepted 17 October 2016; published online 1 February 2017)

Vortex dynamics in the flow past a sphere in a linearly stratified environment is investigated numerically. Simulations are carried out for a flow with Reynolds number of $Re = 3700$ and for several Froude numbers ranging from the unstratified case with $Fr = \infty$ to a highly stratified wake with $Fr = 0.025$. Isosurface of Q criterion is used to elucidate stratification effects on vortical structures near the sphere and in the wake. Vortical structures in the unstratified case are tube-like and show no preference in their orientation. Moderate stratification alters the orientation of vortical structures to streamwise preference but does not change their tube-like form. In strongly stratified cases with $Fr \leq 0.5$, there is strong suppression in vertical motion so that isotropically oriented vortex tubes of approximately circular cross section are replaced by flattened vortex tubes that are horizontally oriented. At $Fr = 0.025$, pancake eddies and surfboard-like inclined structures emerge in the near wake and have a regular streamwise spacing that is associated with the frequency of vortex shedding from the sphere. Enstrophy variance budget is used to analyze the vortical structure dynamics. Increasing stratification generally decreases enstrophy variance for $Fr \geq O(1)$ cases. The flow enters a new regime in strongly stratified cases with $Fr \leq 0.25$: increasing the stratification increases enstrophy variance, especially near the body. Stratification distorts the cross-sectional distribution of enstrophy variance from a circular isotropic shape in the unstratified wake into different shapes, depending on Fr and distance from the sphere, that include (1) elliptical distribution, (2) twin peaks suggestive of two-dimensional vortex shedding, and (3) triple-layer distribution where a relatively low enstrophy layer is sandwiched between the upper and the lower layers with high enstrophy. In the near wake, vortex stretching by fluctuating and mean strain are both responsible for enhancing vorticity. Increasing stratification (decreasing Fr) to $O(1)$ values tends to suppress vortex stretching. Upon further reduction of Fr below 0.25, the vortex stretching takes large values near the sphere and, consequently, enstrophy variance in the near wake increases. The increase in vortex stretching is associated with unsteady, intermittent shedding of the boundary layer from the sides of the sphere in highly stratified wakes with $Fr < 0.25$. *Published by AIP Publishing.* [http://dx.doi.org/10.1063/1.4974503]

I. INTRODUCTION

Turbulence presents a spatially complex distribution of vorticity. Turbulent flow contains a wide range of vortical structures with various length scales and turn-over time scales. The influence of these vortical structures on turbulence dynamics from nonlinear cascade to scalar mixing to kinetic energy dissipation has been the subject of much study but less so in stratified flows. Stratification is ubiquitous in the environment and buoyancy affects the turbulent flows past marine swimmers, underwater submersibles, flying vehicles, underwater topography, islands, and mountains.

Turbulent wakes in stratified fluid have been the subject of experimental study for over 30 yr as summarized below but numerical turbulence-resolving simulations of the wake that include the body are relatively recent. Lin and Pao[1] reviewed experimental studies that showed stratification suppresses vertical motion, promotes downstream horizontal coherent eddies, and enables propagation of internal gravity waves into the far field. Hanazaki[2] numerically simulated stratified flow over a sphere at Reynolds number (Re) of 200 and Froude number $Fr_R \in [0.25\ 200]$ ($Fr_R = U/NR$, where U, N, and R are free stream velocity, buoyancy frequency, and radius of the sphere). Direct numerical simulation (DNS) of Hanazaki[2] provided visualization of downward motion of vertical velocity and isopycnal lines showing a lee wave behind the sphere at low Fr. Chomaz *et al.*[3] experimentally showed that the downward motion induced by stratification delays separation. The downward motion also alters the separation region from circular to a bow-tie shape. Chomaz *et al.*[4] identified four different regimes based on Fr, where $Fr = U/ND$. For $Fr < 0.4$, the wake corresponds to triple-layer flow with two lee waves surrounding a layer of two-dimensional motion. Between Fr of 0.4 and 0.75, the saturated lee wave suppresses the separation region or splits it into two. Between Fr of 0.75 and 2, the wake progressively recovers its behavior in a homogeneous fluid. For Fr larger than 2.25, the near wake is similar to the homogeneous case.

[a]Electronic mail: kchongsi@eng.ucsd.edu
[b]Electronic mail: sarkar@ucsd.edu

RIGHTSLINK

A stratified wake at high Fr exhibits three distinct regions. The first region is the near wake (NW) where the wake spreads uniformly in all dimensions and turbulence behaves as it does in a homogeneous fluid. It is followed by a second non-equilibrium (NEQ) regime identified by Spedding[5] where there is an onset of stratification effect including conversion of stored potential energy to kinetic energy and anisotropy between horizontal and vertical motions. The third region (Q2D) is characterized by the existence of vertically suppressed two-dimensional eddies, the so called "pancake vortices." The formation mechanism of the pancake vortices has been debated. Pao and Kao[6] state that it is due to the helical vortex shed by the sphere that persists into the far wake while Spedding[7] attributes the mechanism to a combination of KH instability and spiral mode instabilities. Bonnier *et al.*[8] and Gourlay *et al.*[9] argue that the existence of pancake vortices does not require coherent structures in the near wake. Later DNS by Dommermuth *et al.*,[10] Brucker and Sarkar,[11] and Diamessis and Spedding[12] also find pancake vortices in their temporal flow model with initial conditions that do not explicitly include coherent structures. Note that the temporal flow model refers to an approximation where the streamwise direction in the computational domain is assumed to be periodic, the Reynolds-averaged statistics evolve in time, and these statistics are obtained by streamwise averaging. The temporal approximation is applicable to a frame moving with the body velocity U and is adequate if the wake deficit is small relative to U and if realistic initial conditions for the flow field can be prescribed. The numerical approach of this paper is a *spatially evolving model* where streamwise periodicity is not assumed and the Reynolds-averaged statistics, computed by temporal averaging, evolve as a function of streamwise distance. Pasquetti[13] avoids *ad hoc* prescription of the initial conditions in a temporal model by first performing body-inclusive spatially evolving simulation and then symmetrically embedding a subdomain from that simulation into a larger domain for the temporal model. Similar to experiments, Pasquetti[13] found that an intermediate NEQ regime was followed by large scale quasi-2D structures in the late wake.

Investigation of coherent structures and vorticity statistics has provided useful information regarding the turbulent wake structure. Yun *et al.*[14] numerically traced vortical structures behind a sphere at $Re = 3700$ and 10^4. Constantinescu and Squires[15] visualized vortical structures using the method of Jeong and Hussain[16] in the subcritical and supercritical regimes, where the boundary layer on the sphere surface is laminar and turbulent, respectively. These studies, however, did not include background density gradient. Spedding[5] visualized vertical vorticity of stratified wake up to $Nt = 1600$ revealing large scale pancake vortices. Spedding[17] examined vortical structure in wakes with $Fr \geq 2$ and stated that most of the late-time properties of long-lived vortex structure are independent of initial Froude number.

Recently Pal *et al.*[18] performed DNS of stratified flow past a sphere at $Re = 3700$ over a wide range of Fr in the range $[0.025, \infty]$. They found that the near wake at $Fr = 0.5$ has very low fluctuation energy but further reduction of Fr to 0.25 and beyond regenerates turbulent fluctuations in the near wake. The turbulent kinetic energy (TKE) in the near wake ($x/D < 20$) of these low-Fr wakes became substantially larger than that in the unstratified case. The simulation data are analyzed in the present paper and new results on the behavior of the small scales are presented by analyzing the behavior of all components of enstrophy and its budget. We also examine the changes in vortex dynamics and coherent structures, identified using the Q-criterion, that are brought about by increased stratification. All prior numerical studies of the vorticity structure in a stratified wake have employed a temporal flow model for the simulations while the present study has the advantage of using a spatial flow model that includes the body. We address the following questions. How does stratification change vortical structures near the body and in the wake? Is there any qualitative difference in terms of enstrophy magnitude and distribution between the moderately and strongly stratified regimes? What are the mechanisms that are responsible for changes in enstrophy (a metric of small-scale fluctuations) induced by stratification?

II. FORMULATION

A. Governing equations

Continuity:

$$\frac{\partial u_i^*}{\partial x_i^*} = 0. \tag{1}$$

Momentum:

$$\frac{\partial u_i^*}{\partial t^*} + u_j^* \frac{\partial u_i^*}{\partial x_j^*} = -\frac{1}{\rho_0}\frac{\partial p^*}{\partial x_i^*} + \nu \frac{\partial^2 u_i^*}{\partial x_j^* \partial x_j^*} - \frac{\tilde{\rho}^*}{\rho_0} g \delta_{i3}. \tag{2}$$

Density:

$$\frac{\partial \rho^*}{\partial t^*} + u_j^* \frac{\partial \rho^*}{\partial x_j^*} = \kappa \frac{\partial^2 \rho^*}{\partial x_j^* \partial x_j^*}. \tag{3}$$

The * superscript denotes dimensional quantities. ν is the kinematic viscosity and κ is the density diffusivity. The density is decomposed into a background density, ρ_0, a linear variation in x_3 direction, $\bar{\rho}^*(x_3)$ and a fluctuation, $\tilde{\rho}^*(x_i, t)$,

$$\rho^* = \rho_0 + \bar{\rho}^*(x_3) + \tilde{\rho}^*(x_i, t), \tag{4}$$

where $\rho^* - \rho_0 \ll \rho_0$. Density variation enters the momentum equation only through the buoyancy term. These equations are non-dimensionalized using U (the free stream velocity), D (the diameter of the sphere), ρ_0, and $C^* = -\partial \bar{\rho}^*(x_3)/\partial x_3^*|_{(t=0)}$

TABLE I. Simulation parameters. The sphere center is at $x = 0$, and the streamwise domain length is split into downstream (L_x^+) and upstream (L_x^-) portions; $L_x = L_x^+ + L_x^-$.

Case	L_x^+/D	L_x^-/D	L_r/D	N_x	N_r
Fr = ∞	80.1	13.8	16.2	4608	632
Fr = 3	80.1	13.8	59.7	4608	692
Fr = 1	80.1	25.7	59.7	4608	692
Fr = 0.5	79.3	39.2	59.7	4608	692
Fr = 0.25	79.3	39.2	59.7	4608	692
Fr = 0.125	79.3	39.2	59.7	4608	692
Fr = 0.05	23.3	39.2	59.7	3072	692
Fr = 0.025	23.3	39.2	59.7	3072	692

RIGHTSLINK

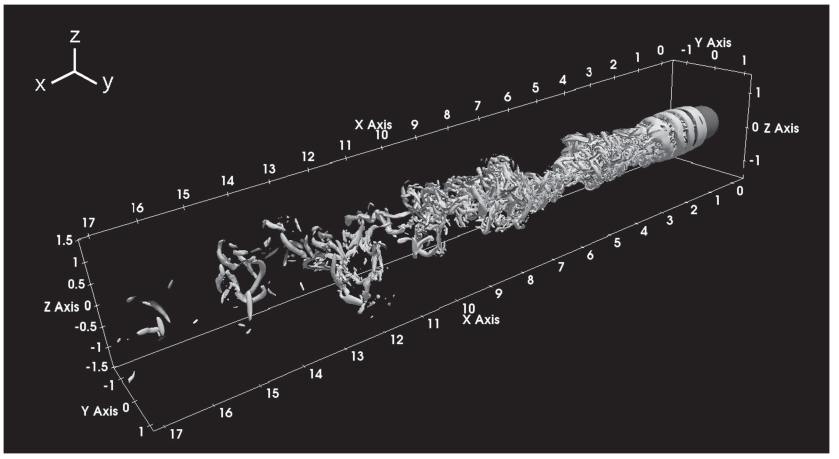

FIG. 1. Iso-surface of Q criterion at Q = 1 for $Fr = \infty$. Note that the sphere center is at $x = 0$, $y = 0$, and $z = 0$.

that denotes the constant vertical gradient of background density. The new non-dimensional variables obtained are

$$t = \frac{t^* U}{D}, \quad x_i = \frac{x_i^*}{D}, \quad u_i = \frac{u_i^*}{U},$$
$$\rho = \frac{\rho^*}{\rho_0}, \quad \tilde{\rho} = \frac{\tilde{\rho}^*}{DC^*}, \quad p = \frac{p^*}{\rho_0 U^2}. \tag{5}$$

Substituting Equation (5) into (1)–(3), we obtain the non-dimensionalized form as follows:

Continuity:

$$\frac{\partial u_i}{\partial x_i} = 0. \tag{6}$$

Momentum:

$$\frac{\partial u_i}{\partial t} + u_j \frac{\partial u_i}{\partial x_j} = -\frac{\partial p}{\partial x_i} + \frac{1}{Re}\frac{\partial^2 u_i}{\partial x_j \partial x_j} - \frac{1}{Fr^2}\tilde{\rho}\delta_{i3}. \tag{7}$$

Density:

$$\frac{\partial \rho}{\partial t} + u_j \frac{\partial \rho}{\partial x_j} = \frac{1}{RePr}\frac{\partial^2 \rho}{\partial x_j \partial x_j}. \tag{8}$$

Here, the relevant non-dimensional parameters are as follows: the Reynolds number, $Re = UD/\nu$, the Prandtl number, $Pr = \nu/\kappa$, and the Froude number, $Fr = U/(ND)$, where N is the buoyancy frequency defined by $N = [-gC^*/\rho_0]^{1/2}$. In the following discussion, all variables referenced are non-dimensional unless otherwise noted.

B. Numerical scheme

The governing equations (6)–(8) are solved numerically using direct numerical simulation (DNS) in a cylindrical coordinate system on staggered grids. The sphere is represented by the immersed boundary method of Yang and Balaras,[19] and Balaras.[20] The governing equations are marched using a combination of explicit and implicit schemes. Implicit marching by the second order Crank-Nicolson (CN) scheme is performed for the viscous terms to alleviate the stiffness of the discretized system. The remaining terms are marched explicitly using a third-order Runge-Kutta (RK3) scheme. The periodic boundary condition in the azimuthal direction reduces the discretized Poisson equation into inversion of a pentadiagonal matrix. The pentadiagonal matrix system is solved using a direct solver, Yang and Balaras.[19] Inflow and convective outflow boundary conditions are applied at the inlet and outlet of the domain. In order to control spurious reflections from internal waves and other disturbances propagating out of the domain, sponge regions are employed near the free stream and inlet boundaries where the following relaxation terms are added to the governing equations:

$$-\phi(x_i)[u_i(x_i,t) - U_i], \quad -\phi(x_i)[\rho(x_i,t) - \rho_\infty(x_3)]. \tag{9}$$

The sponge layer takes the form of a Rayleigh damping function which is designed in such a way that it gradually relaxes the velocities and density to their respective values at the boundaries. Here U_i is the freestream velocity and $\rho_\infty(x_3)$ is the density of the stratified background. This is accomplished by

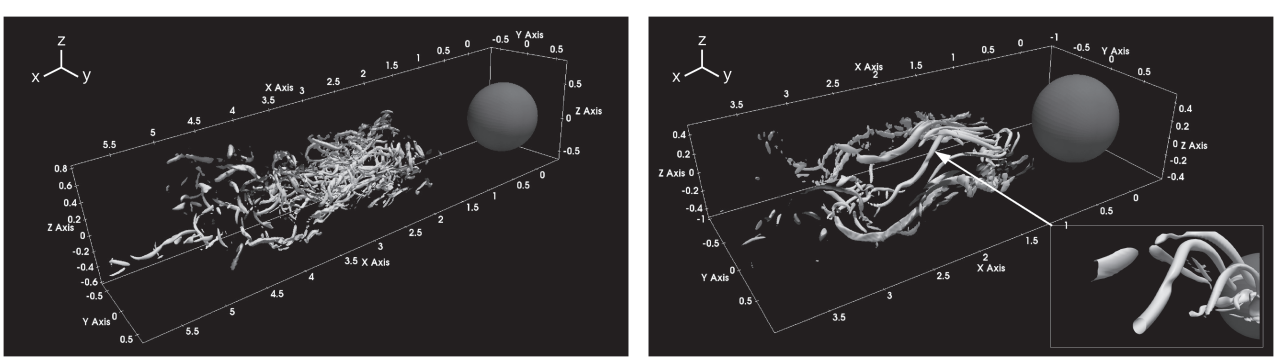

FIG. 2. Iso-surface of Q criterion at Q = 50 for $Fr = \infty$ (left) and $Fr = 1$ (right). Inset on right panel shows the circular cross section of the vortex tube.

RIGHTSLINK

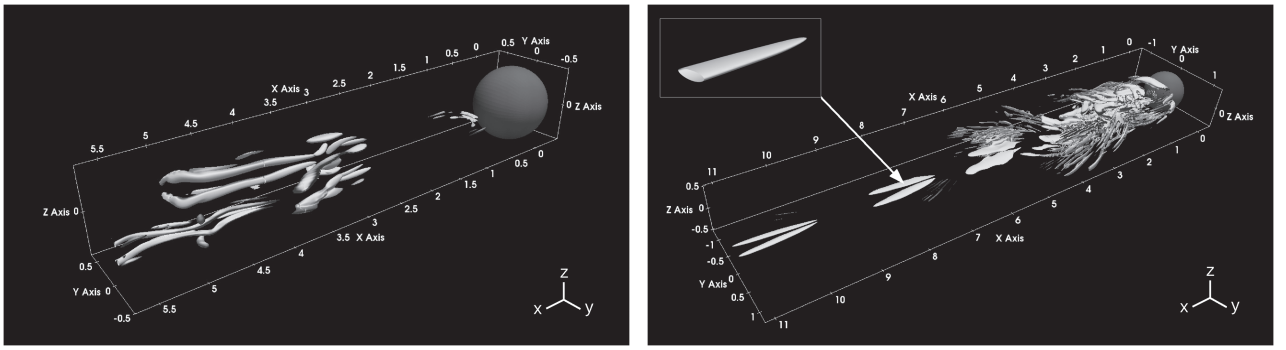

FIG. 3. Iso-surface of Q criterion at Q = 5 for $Fr = 0.5$ (left) and for $Fr = 0.125$ (right). Inset on right shows the elliptical cross section of the vortex tube in the strongly stratified regime.

adding the explicit damping terms of Equation (9) to the right hand side of Equations (7) and (8), respectively. The variable $\phi(x_i)$ is constructed such that it increases quadratically from $\phi = 0$ to $\phi = 1$ over a sponge region of thickness 10 grid points at the inflow and at the freestream boundaries.

C. Parameters

Table I shows parameters for the eight simulations that range from an unstratified case to the highly stratified case with $Fr = 0.025$. All simulations are performed with $Re = 3700$ and the number of points in the azimuthal direction is chosen to be $N_\theta = 128$. The choice of $Re = 3700$ allows validation against DNS of unstratified flow past a sphere by Rodriguez *et al.*[21] The choice of $Pr = 1$ is justified by de Stadler *et al.*[22] L_x/D and L_r/D are domain sizes in the streamwise and radial directions, respectively. Domain size in the radial direction and in the upstream direction for all stratified cases is enlarged to allow free propagation of internal gravity waves. The total number of grid points is approximately 400×10^6. Grid stretching is used in radial and streamwise directions to concentrate points near the sphere surface in order to resolve the laminar boundary layer. The domain is decomposed only in the streamwise direction which reduces communication time between processors as compared to three-dimensional decomposition. Each simulation requires approximately 500 h run time on 512 processors. Temporal averaging of data to compute statistics is performed over 80-100 time units or approximately a single flow-through time unit after a statistical steady-state.

III. METHODS OF DATA ANALYSIS

The flow is statistically inhomogeneous in all directions. Thus, Reynolds-averaged statistics are obtained by averaging solely over time. Vorticity is computed in cylindrical coordinates prior to transformation into the Cartesian coordinate. The total enstrophy can be decomposed into mean and fluctuating components. In the present paper, we examine the fluctuating enstrophy which hereafter is simply called enstrophy (the second term of the rhs in Equation (11)). Reynolds average is denoted with overline. Three dimensional visualization of vortices is done using the Q-criterion of Hunt *et al.*[23] which defines a vortex by the region where the rate of rotation tensor, Ω_{ij}, exceeds strain rate tensor, S_{ij}. Large positive Q implies strong swirling motion,

$$u_i = \overline{u_i} + u_i', \quad \rho_i = \overline{\rho_i} + \rho_i', \quad \tilde{\rho}_i = \overline{\tilde{\rho}_i} + \tilde{\rho}_i', \quad p_i = \overline{p_i} + p_i', \tag{10}$$

$$\frac{1}{2}\left(\overline{\omega_i \omega_i}\right) = \frac{1}{2}\left(\overline{\omega_i}\,\overline{\omega_i}\right) + \frac{1}{2}\left(\overline{\omega_i' \omega_i'}\right), \quad \omega_i = \epsilon_{ijk}\frac{\partial u_k}{\partial x_j} \tag{11}$$

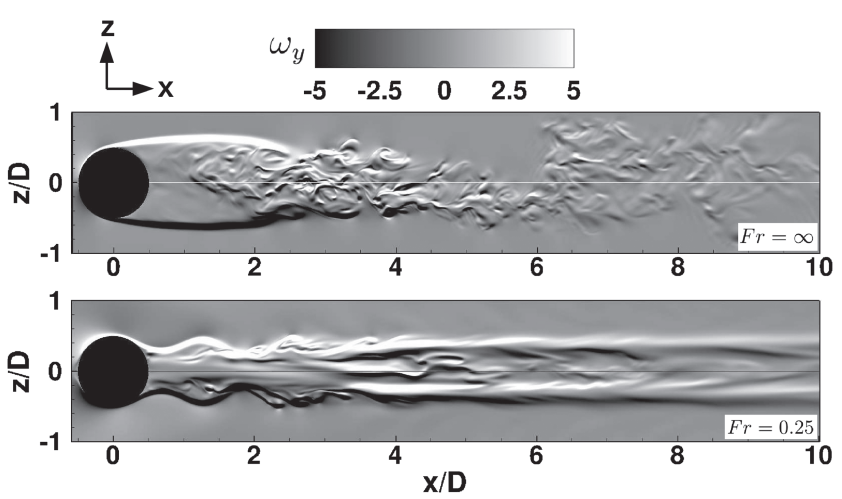

FIG. 4. Side view azimuthal vorticity (ω_y) for $Fr = \infty$ (top) and $Fr = 0.25$ (bottom).

RIGHTSLINK

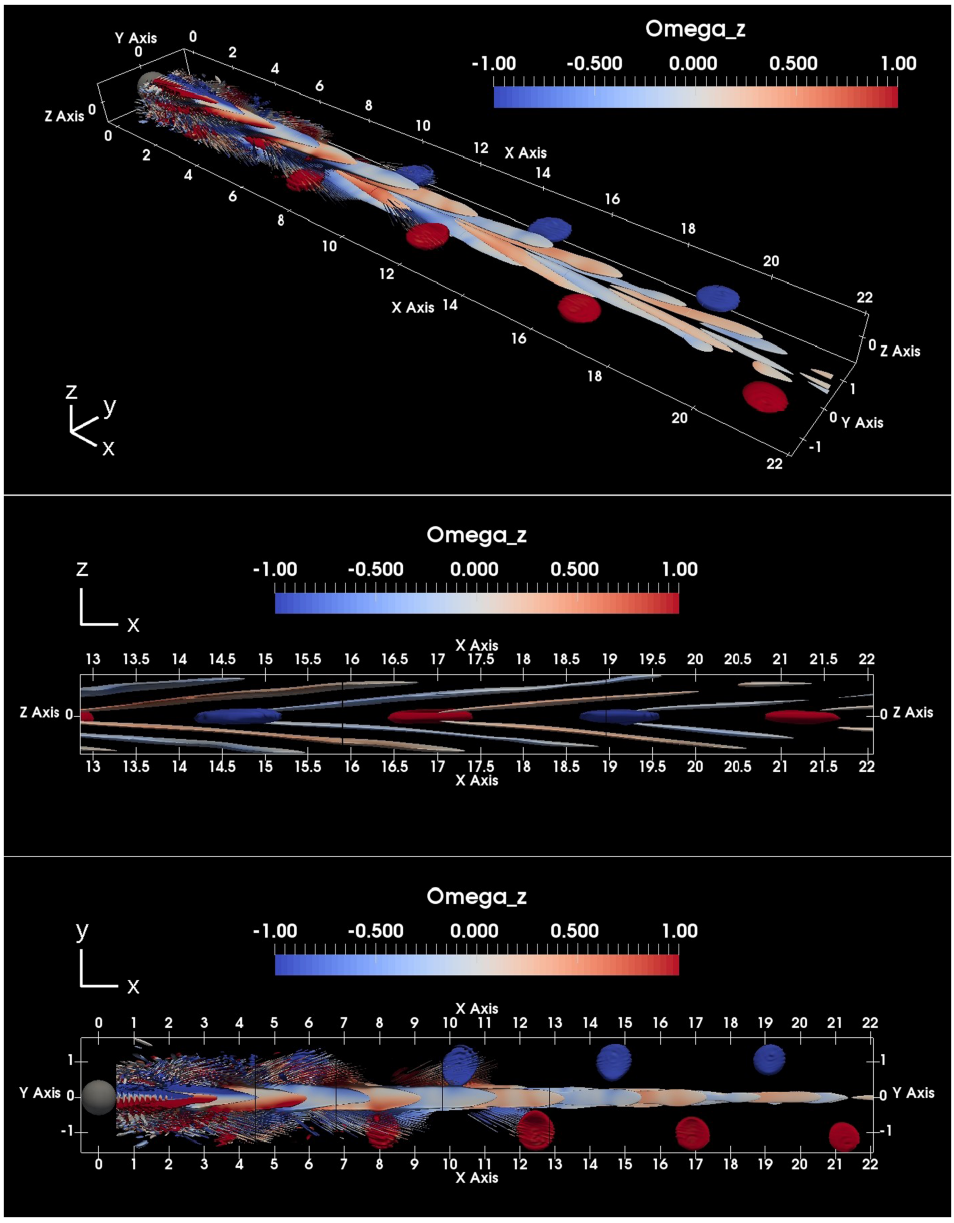

FIG. 5. Coherent structures in a strongly stratified wake (Fr = 0.025) visualized with the isosurface of Q = 0.25. Top panel is a perspective of the wake with the sphere at the upper left corner. Middle panel is a side view (flow from left to right) and bottom panel is a top view.

$$Q = \frac{1}{2}(|\mathbf{\Omega}|^2 - |\mathbf{S}|^2), \quad \Omega_{ij} = \frac{1}{2}\left(\frac{\partial u_i}{\partial x_j} - \frac{\partial u_j}{\partial x_i}\right), \quad S_{ij} = \frac{1}{2}\left(\frac{\partial u_i}{\partial x_j} + \frac{\partial u_j}{\partial x_i}\right). \tag{12}$$

IV. RESULTS

The numerical method and grid resolution of the present DNS were validated using experimental measurements and numerical results available in the literature by Pal *et al.*[18] Comparison of nondimensional vortex shedding frequency, $St = fD/U$, separation angle, φ_s, drag coefficient, C_d, and rearward stagnation pressure coefficient, C_{pb}, agrees well with the previous investigations[14,15,21,24–28] as discussed by Pal *et al.*[18]

A. Wake vortices

1. Vortex configuration

Figure 1 visualizes instantaneous vortical structures in the wake using the Q-criterion at Q = 1 for the unstratified case.

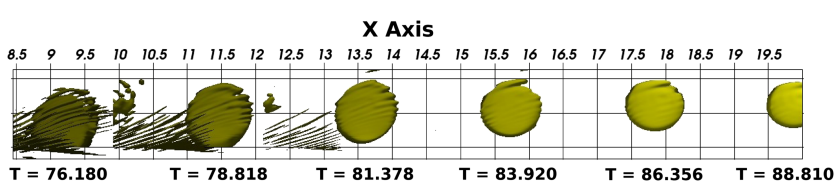

FIG. 6. Location of a pancake eddy for Fr = 0.025 versus time.

RIGHTSLINK

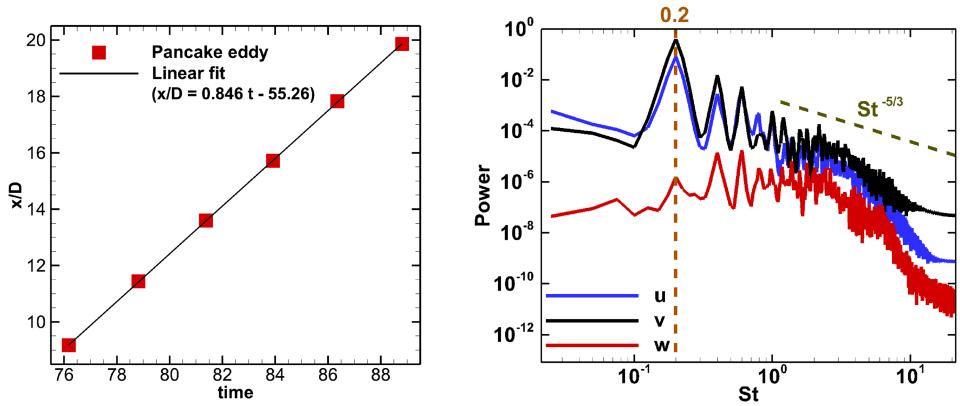

FIG. 7. Location of a pancake eddy vs time (left) and power spectra of velocity components for $Fr = 0.025$ at $x/D = 2.19$, $y/D = 0.51$, and $z = 0$ (right).

Since Q, defined by Equation (12), represents a region where the rate of rotation tensor Ω_{ij} exceeds the strain rate tensor S_{ij}, a high value of Q signifies intense rotation of fluid elements. Close to the body, vortex rings are shed from the sphere in the unstratified wake (Figure 1). These rings remain circular before breaking down at around $x/D = 2.4$, Rodriguez *et al.*[21] Immediately downstream of the transition, a bundle of entangled vortical structures emerges. These vortices are tube-like structures with high length-to-diameter aspect ratio, the so-called vortex tube. For both Fr, even though the vortex tubes in general do not have directional preference, the subset of streamwise-oriented tubular structures has high-magnitude streamwise vorticity and no preference for other vorticity components. In Figure 1, the density of vortex tubes per unit volume based on $Q = 1$ decreases significantly after $x/D \approx 7$.

Figure 2 shows vortices at a higher magnitude of Q = 50. At this level of Q, vortical structures in the unstratified $Fr = \infty$ wake are present in the region $1.5 < x/D < 5$, while they are absent elsewhere. The fact that the strength (Q) of the vortex tubes spanning $1.5 < x/D < 5$ is higher than that of vortices shed from the body indicates that vortex shedding is not the only source of vorticity. The mechanisms generating vorticity will be explained later in Sec. IV C. Streaky structures closer to the sphere seem to have preferred orientation in the streamwise direction while this preference is lost away from the body. Stratification at $Fr = 1$, Figure 2 (right), elongates the vortex tubes and thus increases their aspect ratio. The vortical structures have a vertical undulation owing to a steady lee wave pattern behind the body. The number density of vortical structures is significantly smaller than that in the unstratified wake showing suppression of enstrophy (will be quantified later) at this level of stratification. Stratification at $Fr = 0.5$ confines vortex tubes to streamwise-oriented regions as shown in Figure 3. Two pairs of streaks are observed having their size longer than the sphere's diameter. That fluctuating enstrophy is suppressed by stratification is evident since vortical structures at $Fr = 0.5$ are barely observed even with Q = 5.

While vortical structures depicted by the isosurface of Q for weak stratification ($Fr \geq 0.5$) bear some similarities to the unstratified case in terms of size, aspect ratio, and orientation, structures at stronger stratification ($Fr = 0.125$) shown in Figure 3 (right) are significantly different. From Figure 3 (right), immediately after the sphere there is a stack of long thin flattened tubes that alternate on either side of the vertical center-plane. This is due to quasi two-dimensional vortex shedding from the sides of the sphere.

The azimuthal vorticity, ω_y, is organized into a triple layer as shown by the side view of the $Fr = 0.25$ case in Figure 4. The lee wave is apparent in the stratified case and the variability of vorticity is diminished. The vertical wake height is narrower in comparison to the unstratified case and the wake is bounded by the top and bottom shear layers which exhibit

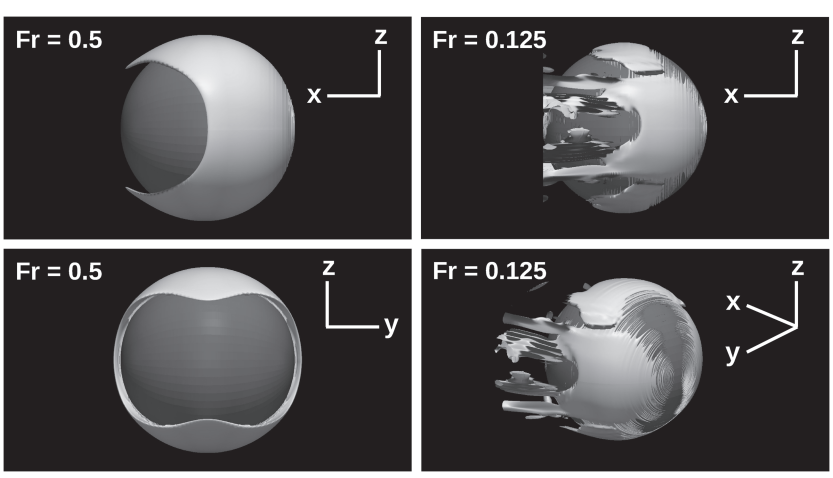

FIG. 8. Isosurface of Q criterion used to examine flow separation.

RIGHTSLINK

vertical undulations impressed by a steady lee wave pattern but little turbulence. The middle layer contains horizontal strips of vorticity that are thin in the vertical. The isosurface of Q at $Fr = 0.25$ is similar to that of $Fr = 0.125$ and is not shown here.

The quasi-2D regime is a feature of the far wake, appearing at $x/D \approx 1000$ or $Nt \approx 250$ in the moderately stratified $Fr = 4$ wake simulated by Brucker and Sarkar[11] in a temporal flow model. When the stratification is very high, pancake vortices emerge in the near wake. Isosurface of Q = 0.25 in the perspective view of Figure 5 (top) reveals two types of organized structures, both are thin in the vertical. Pancake vortices which take the form of discs are clear and the first pancake eddy is seen in the perspective view of the top panel at $x/D \approx 6$ which corresponds to $Nt = 6/Fr = 240$ which is close to the value of $Nt \approx 250$ quoted by Brucker and Sarkar.[11] While the pancake vortices are located off the center line, there are "surfboard" structures sequentially located closer to the middle. The side view (Figure 5 middle) shows that, while the pancakes are located on the horizontal center plane, the surfboard-like structures are not horizontally oriented and their leading edges are located at the same x/D location as of the pancake eddies. In the side view, each surfboard pair appears as a V with the vertex of the V coincident with the pancake. An average distance between the pancake eddies is $x/D = 4.41$ according to Figure 5 (bottom). The advection velocity of a pancake is obtained by tracking an eddy through time as shown in Figure 6.

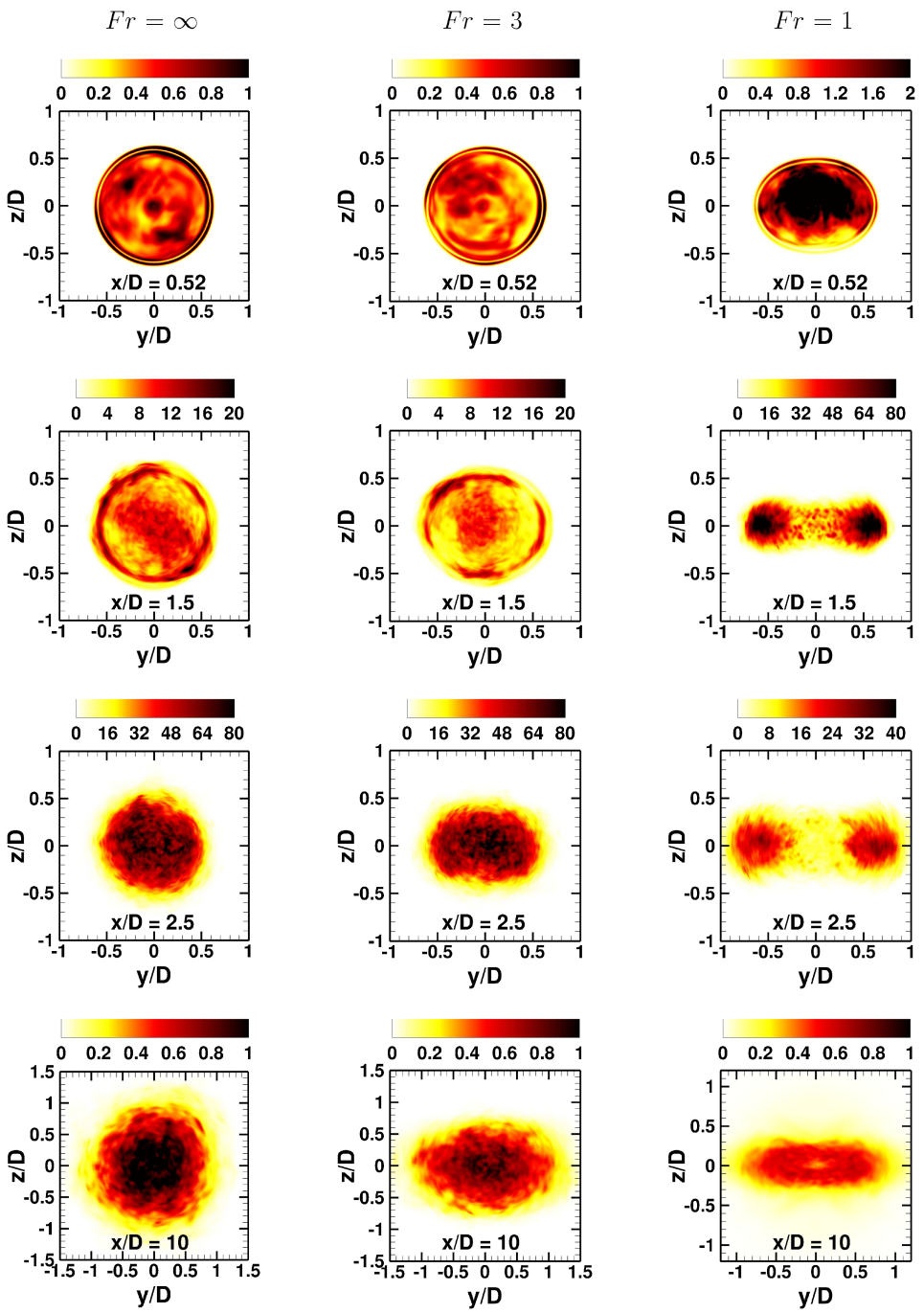

FIG. 9. Enstrophy, $0.5\overline{(\omega_i'\omega_i')}$, plotted over a transverse cross section at various streamwise locations. Cases with $Fr = \infty$, 3, and 1 are shown.

RIGHTSLINK

Figure 7 (left) reveals an advection velocity of 0.846. The spacing between two subsequent pancake eddies and this estimate of advection velocity allows conversion to temporal frequency of the pancake eddy, leading to a Strouhal number of $St = fD/U = 0.192$. The primary peak in the streamwise and spanwise velocities power spectra (Figure 7 right panel) is at $St \approx 0.2$. Therefore, the origin of these pancake eddies is shedding of boundary layer vorticity from the sides of the sphere (similar to the Karman vortex street of a cylinder). This frequency is close to the shedding frequency of flow past a cylinder at ($St = 0.208$) reported in the work of Parnaudeau *et al.*[29] The surfboard structures are shed from the sphere with the same frequency as of the pancakes. Inspection of the flow near the sphere suggests that the surfboards are an interaction of the top and bottom separated boundary layers with the horizontal vortex shedding.

Another kinematic aspect of the pancakes and of the surfboards apart from their convective translation is their rotational direction. The isosurface of Q is colored with vertical vorticity. The pancake disks originate from quasi–2D shedding of the boundary layer in the horizontal center plane. The shedding occurs from alternate sides of the sphere and the sign of the vertical vorticity of a pancake disk depends on the side of the centerline that it occupies. Two surfboard structures that form a "V" in Figure 5 (middle) have the same orientation of vertical vorticity as the pancake at the vertex of the V suggesting continuity of vortex lines at the leading edge of the V. The

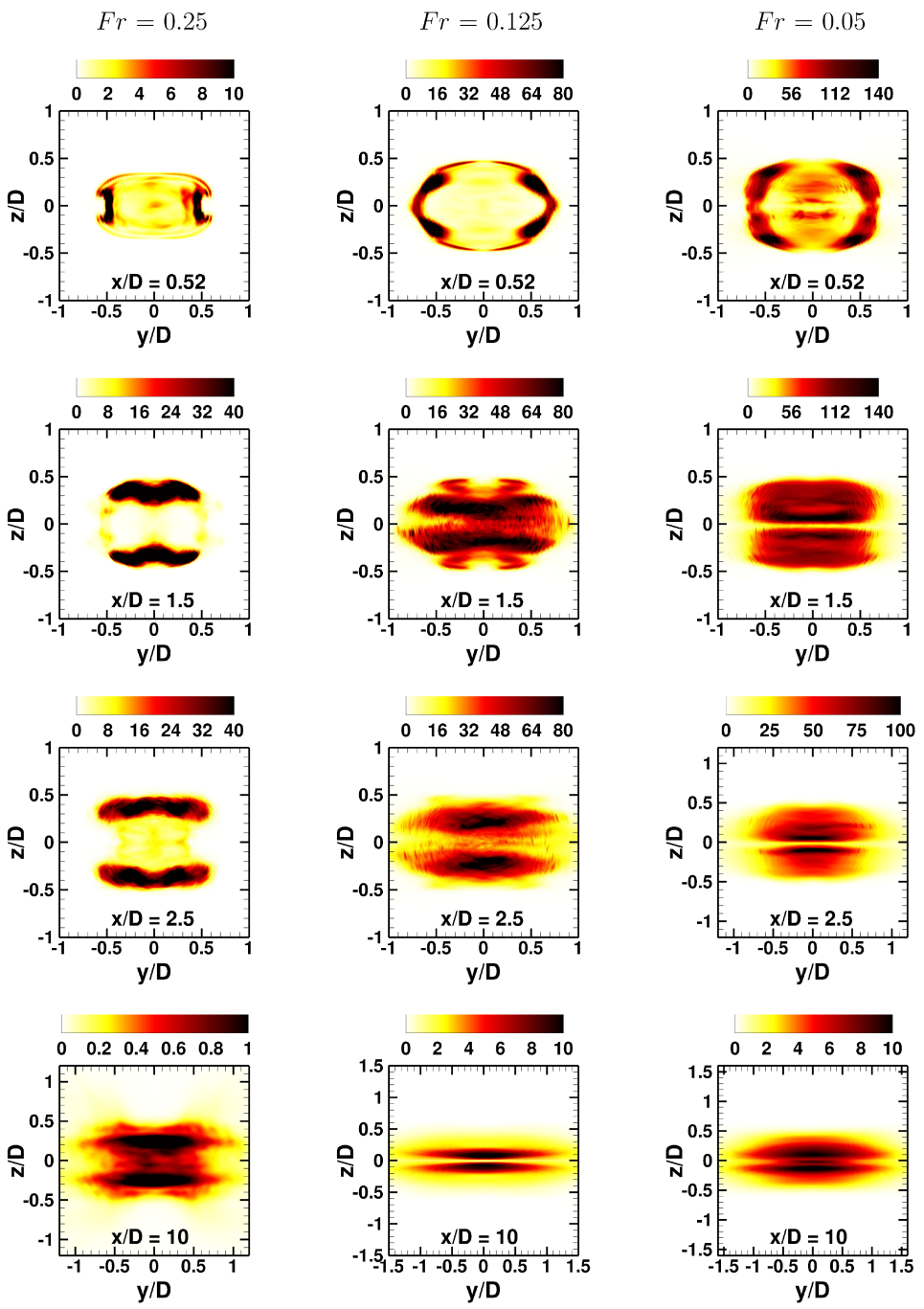

FIG. 10. Enstrophy, $0.5\overline{(\omega_i'\omega_i')}$, plotted over a transverse cross section at various streamwise locations. Cases with $Fr = 0.25$, 0.125, and 0.05 are shown.

RIGHTSLINK

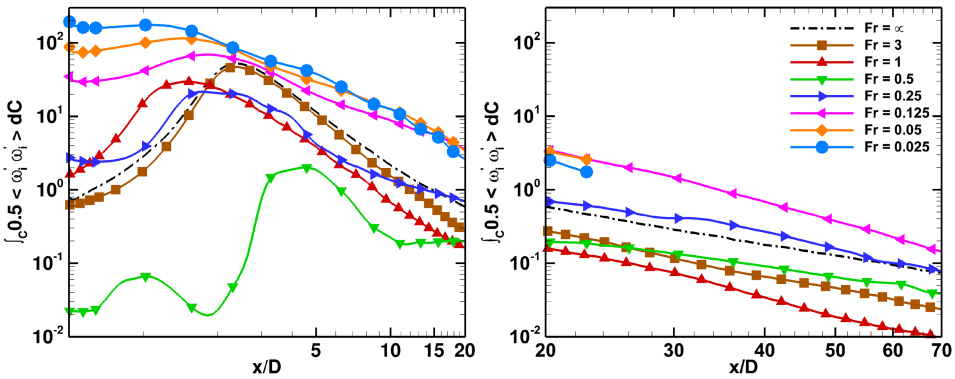

FIG. 11. Streamwise variation of area-integrated enstrophy.

vertical vorticity amplitude of these surfboards is, however, smaller than that of the pancake disks. Overall, the distribution of vorticity is indicative of a sinuous instability mode.

2. Separation

While there are quantitative changes in how the incoming flow goes past the sphere under different levels of stratification, the cases of $Fr = 0.5$ and 0.125 shown in Figure 8 are sufficient to illustrate the qualitative changes induced by buoyancy on the flow at the sphere and its separation. At moderate Fr, the incoming flow has enough kinetic energy to go above and below the sphere which can be seen from the smooth and continuous isosurface of Q at $Fr = 0.5$. There is a difference with respect to the axisymmetric separation in the unstratified case. Stratification delays separation at the top and bottom of the sphere with respect to its sides. Due to conversion of stored potential energy to kinetic energy, fluid at the top and bottom regions gains momentum which helps the boundary layer overcome the adverse pressure gradient and remain attached to the surface further downstream than in the horizontal plane. This results in the delay of separation in the vertical plane. The separation line viewed from the rear (bottom-left panel of Figure 8) has a bow-tie shape. At sufficiently low Fr, there is another qualitative change: flow blocking, i.e., the incoming flow does not have enough kinetic energy to go past the top and bottom points of the sphere. Therefore, the flow is forced to go around the sphere for $Fr = 0.125$ as shown by the absence of Q isosurface in the central region on the frontward-facing surface of the sphere (Figure 8, bottom right panel). The boundary layer at $Fr = 0.125$ is shed from the sides of the sphere (Figure 8, top and bottom right panels).

3. Spatial distribution of enstrophy variance

Figure 9 shows the spatial distribution of enstrophy at different downstream locations for Fr = ∞, 3, and 1. Beyond $x/D = 2.5$, the enstrophy in the core of the wake tends to decrease with decreasing Fr until $Fr = 0.5$ (not plotted) where the enstrophy is rather small, about 1% of that at $Fr = \infty$. The distribution of enstrophy also changes among cases. Consider $x/D = 0.52$ (top panel). For $Fr = \infty$, there is a thin circular ring of high enstrophy associated with the separating boundary layer, also seen as a sequence of vortex rings in the visualization of Q (Figure 1). The separating boundary layer forms an unstable ring-like shear layer that has enhanced enstrophy. As stratification increases (Fr decreases), the boundary of the region with relatively high enstrophy starts distorting from a circle to an ellipse. This non-circular cross section very close to the sphere is consistent with the previous discussion of boundary layer separation occurring at different angles as measured from the sphere forward stagnation point. At $x/D = 0.52$, the $Fr = 1$ case shows the highest enstrophy among the three cases which can also be surmised from the isosurface of Q = 50 where intense swirling vortex tubes move slightly closer to the sphere as compared to $Fr = \infty$ in Figure 2.

The fluctuating enstrophy increases moving downstream to $x/D = 1.5$. While peak enstrophy still resides at the periphery, there is significant enstrophy in the core associated with the recirculating flow and unsteady, flapping shear layer. Stratification causes downward motion behind the sphere keeping

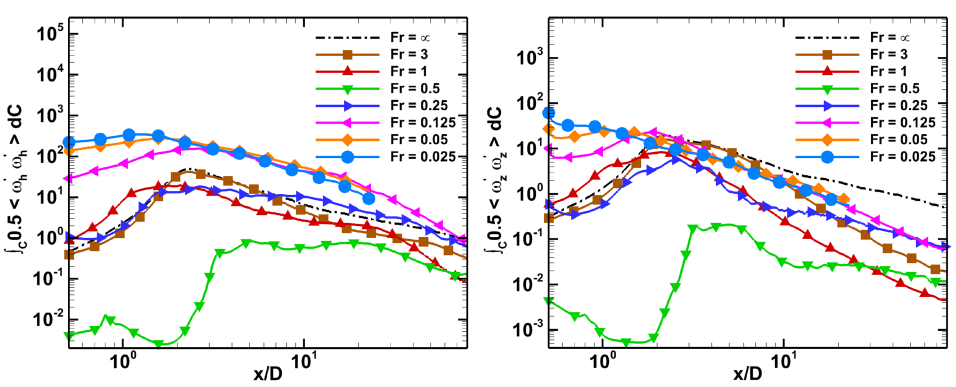

FIG. 12. Partition of area-integrated enstrophy into (a) horizontal component and (b) vertical component.

RIGHTSLINK

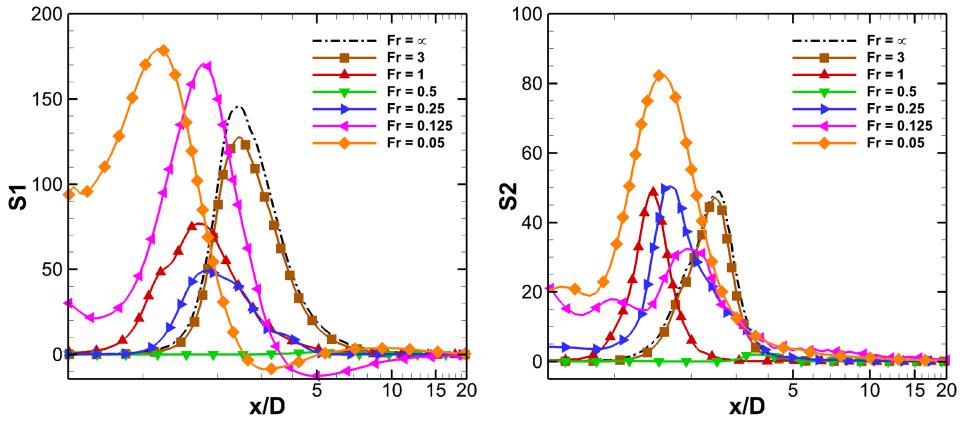

FIG. 13. Cross-sectional integration of stretching term S1 (left) and S2 (right).

relatively high enstrophy closer to the sphere. Moving downstream, the buoyancy-induced anisotropy of cross-sectional enstrophy becomes more pronounced. At $x/D = 1.5$, the $Fr = 1$ cases loses the signature of the vortex ring and, instead, has a dumbbell shape with two local peaks, one on each side of the centerline. These two blobs of enstrophy are approximately 4 times larger in magnitude compared with Fr = ∞ and 3. At $x/D = 2.5$, the enstrophy increases for $Fr = \infty$ and $Fr = 3$ while it fades for $Fr = 1$. By $x/D = 10$ (bottom panel), the two separated peaks of enstrophy are no longer prominent in the $Fr = 1$ wake. Although the enstrophy increases rapidly near the body for $Fr = 1$, stratification at this level suppresses small-scale turbulence after $x/D = 1.5$ according to Figure 9.

Figure 10 shows cross-sectional enstrophy at low Fr of 0.25, 0.125, and 0.05. There is a striking increase of enstrophy in these low-Fr cases relative to the moderate-Fr cases of Figure 9. This implies that small scale fluctuations reappear when Fr decreases beyond 0.25. Furthermore, the distribution of enstrophy is also different in this low-Fr regime relative to that at higher Fr. The flow separates from the sides of the sphere leading to intensified vertical side lobes of vorticity at $x/D = 0.52$. The separated shear layer responds to stratification by developing instabilities with small vertical scale as was seen in the Q-visualizations and also flaps unsteadily (more so in the $Fr = 0.125$ and 0.05 cases) in the horizontal plane. As a result the enstrophy variance takes the form of a horizontally oriented triple layer: there are two outer layers with high enstrophy and a central layer with low enstrophy. The aspect ratio (horizontal to vertical) of these layers becomes progressively larger with increasing Fr.

B. Area-integrated values of enstrophy and its components

The enstrophy integrated over the y-z cross section is shown in Figure 11 for different Fr. In all cases the enstrophy increases, reaches a maximum close to the sphere surface, and then decays. In the low- or moderate-stratification regime with $Fr \geq O(1)$, the effect of buoyancy is to reduce enstrophy. The onset of the stratification effect scales as Nx/D so that the deviation of enstrophy relative to the unstratified case in the $Fr = 3$ wake occurs further downstream than in the $Fr = 1$ case. The value of $Fr = 0.5$ appears to be a critical Fr where the integrated enstrophy in the near wake ($x/D < 20$) is the smallest among all cases.

There is a qualitative change in the stratification effect on enstrophy when Fr decreases below 0.5, namely, the integrated enstrophy near the body ($x/D < 2$) monotonically increases with decreasing Fr. As discussed previously, the boundary layer sheds in a two-dimensional manner in this low-Fr regime; furthermore, vortices are shed unsteadily in the horizontal plane from various vertical locations, develop instabilities with small vertical scale, U/N, and also flap unsteadily in the horizontal plane. These aspects of unsteady motion create a wide range of scales of motion explaining why the enstrophy near the body increases again once $Fr < 0.5$.

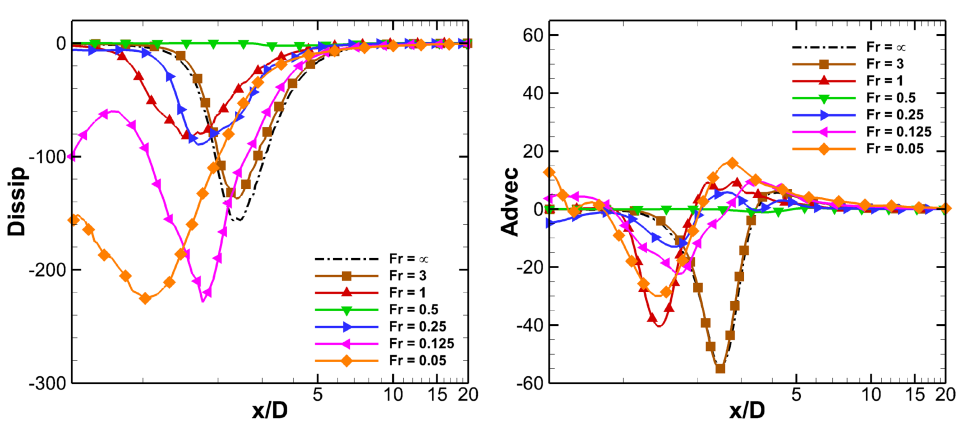

FIG. 14. Cross-sectional integration of dissipation (left) and advection (right).

RIGHTSLINK

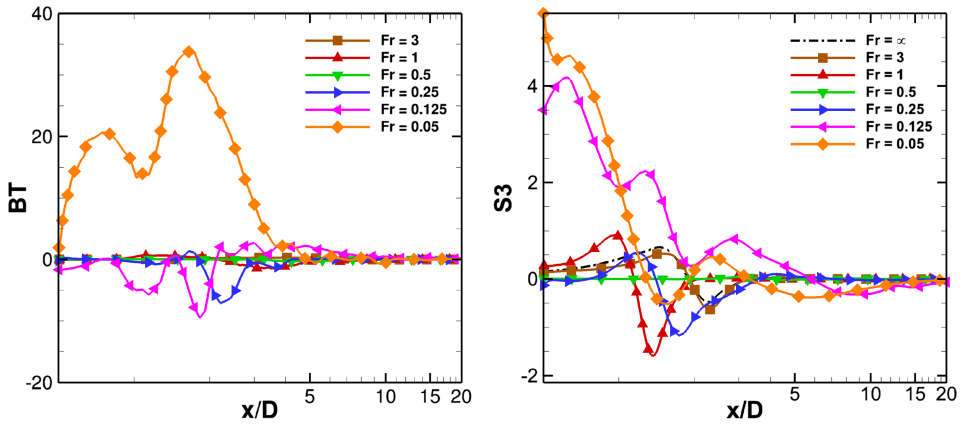

FIG. 15. Cross-sectional integration of baroclinic torque (left) and stretching term S3 (right).

The enstrophy near the body ($x/D < 2$) in the low-Fr cases with $Fr \leq 0.125$ exceeds the corresponding values in the unstratified case substantially, by 1-2 orders of magnitude. There is a rapid rise of enstrophy in the unstratified case which brings its value close to that in the low-Fr regime soon after. However, the relatively rapid spread of the unstratified wake thickness causes a corresponding decrease in enstrophy so that, for $10 < x/D < 70$, the unstratified wake has lower enstrophy than these low-Fr cases. This is in contrast to the situation in the $Fr \geq O(1)$ regime where the unstratified wake has larger enstrophy for $10 < x/D < 70$.

Figure 12 shows decomposition of area-integrated fluctuating enstrophy into vertical (ω_z') and horizontal (ω_h') components. Since ω_x' and ω_y' components behave similarly, both contributions are lumped together in that of ω_h'. The behavior of the unstratified case (black dashed-dotted line) shows that there is little difference between the evolution of horizontal and vertical components. It was shown in Figure 11 that the low-Fr cases with $Fr \leq 0.125$ have larger enstrophy relative to the unstratified case. This remains true for ω_h', but only very near the body ($x/D < 2.5$) in the case of ω_z'. The reason for the similar behavior of ω_z' and ω_h' for $x/D < 2.5$ is that vortex shedding from the side of the sphere (observed in Figures 9 and 10) and subsequent instabilities of the shed vorticity layers increase all components of fluctuating vorticity for $x/D < 2.5$. However the stabilizing effect of buoyancy acts further downstream so that the contribution of the vertical component in all stratified wake simulations tends to decrease faster than the unstratified case at $x/D \approx 4$.

C. Enstrophy mechanisms

The vortex dynamics is analyzed by means of Equation (13) below for the enstrophy variance. Each term is computed at statistical steady-state and the temporal derivative term thus vanishes. The interesting aspect of this equation is whether each term behaves as a source or as a sink of enstrophy. At sufficiently high Re, the dominant source term for the enstrophy equation is stretching by turbulent vorticity ($S1$) and the dominant sink term is dissipation ($DISSIP$), Tennekes and Lumley.[30] Vortex stretching underpins the energy cascade from large to small scales. The strongly positive values of $S1$ in Figure 13 imply that stretching outweighs compression of vortex lines and the net effect of the strain field is to create enstrophy, Tennekes and Lumley.[30]

Consider the unstratified case first. The dominance of stretching and dissipation plotted in Figures 13 and 14, respectively, is clear. Among the three stretching terms, stretching by fluctuating strain ($S1$) is dominant, stretching by mean strain ($S2$) is substantial while stretching of mean vorticity by fluctuating strain ($S3$) (Figure 15, right) is the smallest. Recall that, although there were intense vortical structures (Q = 50) in Figure 2 between $1.5 < x/D < 5$, they were absent near the sphere for $x/D < 1.5$. It is the large positive value of the vortex stretching terms ($S1$ and $S2$) in $1.5 < x/D < 5$ that enables the formation of these large-Q structures. Viscous dissipation ($DISSIP$) is the dominant sink for enstrophy while advection by mean ($ADVEC$) tends to redistribute enstrophy from the region near peak enstrophy. The other terms are at least an order of magnitude less than $S1$, $S2$, $ADVEC$, $DISSIP$ as well described by the order of magnitude analysis of Tennekes and Lumley,[30]

$$\begin{aligned}\frac{\partial}{\partial t}\left(\frac{1}{2}\overline{\omega_i'\omega_i'}\right) &= -\overline{u_j}\frac{\partial}{\partial x_j}\left(\frac{1}{2}\overline{\omega_i'\omega_i'}\right) - \overline{u_j'\omega_i'}\frac{\partial\overline{\omega_i}}{\partial x_j} \\ &\quad - \frac{1}{2}\frac{\partial}{\partial x_j}\left(\overline{u_j'\omega_i'\omega_i'}\right) + \overline{\omega_i'\omega_j's_{ij}'} + \overline{\omega_i'\omega_j'}\,\overline{S_{ij}} \\ &\quad + \overline{\omega_j}\overline{\omega_i's_{ij}'} + \frac{1}{Re}\frac{\partial^2}{\partial x_j\partial x_j}\left(\frac{1}{2}\overline{\omega_i'\omega_i'}\right) - \frac{1}{Re}\overline{\frac{\partial\omega_i'}{\partial x_j}\frac{\partial\omega_i'}{\partial x_j}} \\ &\quad - \frac{\delta_{k3}}{Fr^2}\varepsilon_{ijk}\overline{\omega_i'\frac{\partial\rho'}{\partial x_j}}. \end{aligned} \tag{13}$$

The physical meaning of each term is as follows:

$$\frac{\partial}{\partial t}\left(\frac{1}{2}\overline{\omega_i'\omega_i'}\right) : \text{Rate of change of fluctuating enstrophy } (DDT),$$

RIGHTSLINK

$$-\overline{u_j}\frac{\partial}{\partial x_j}\left(\frac{1}{2}\overline{\omega_i'\omega_i'}\right) : \text{Advection by mean } (ADVEC),$$

$$-\overline{u_j'\omega_i'}\frac{\partial\overline{\omega_i}}{\partial x_j} : \text{Production by mean gradient of vorticity } (PROD),$$

$$-\frac{1}{2}\frac{\partial}{\partial x_j}\left(\overline{u_j'\omega_i'\omega_i'}\right) : \text{Diffusion by turbulence } (TDIFF),$$

$$\overline{\omega_i'\omega_j's_{ij}'} : \text{Stretching/tilting of vorticity fluctuation by fluctuating strain } (S1),$$

$$\overline{\omega_i'\omega_j'}\,\overline{S_{ij}} : \text{Stretching/tilting of vorticity fluctuation by mean strain } (S2),$$

$$\overline{\omega_j}\overline{\omega'_i s'_{ij}} : \text{Stretching/tilting of mean vorticity by fluctuating strain } (S3),$$

$$\frac{1}{Re}\frac{\partial^2}{\partial x_j\partial x_j}\left(\frac{1}{2}\overline{\omega_i'\omega_i'}\right) : \text{Diffusion by viscosity } (VDIFF),$$

$$-\frac{1}{Re}\overline{\frac{\partial\omega_i'}{\partial x_j}\frac{\partial\omega_i'}{\partial x_j}} : \text{Dissipation } (DISSIP),$$

$$-\frac{\delta_{k3}}{Fr^2}\varepsilon_{ijk}\overline{\omega_i'\frac{\partial\rho'}{\partial x_j}} : \text{Baroclinic torque } (BT).$$

Buoyancy significantly affects the distribution and magnitude of enstrophy as has been discussed in Secs. IV A and IV B, e.g., Sec. IV B shows that area-integrated enstrophy generally decreases with increasing stratification in moderately stratified wakes with $Fr = O(1)$ and generally increases with increasing stratification for highly stratified wakes with $Fr \leq 0.125$. Quantification of Equation (13) allows examination of the underlying reason for the stratification effect observed in the simulations. Surprisingly, the area-integrated baroclinic torque (BT) is found to be relatively small (Figure 15, left) and not the primary reason. Rather it is the implicit effect of buoyancy on vortex stretching as elaborated below.

Figure 13 shows that vortex stretching tends to decrease when the stratification increases as Fr is reduced to $O(1)$ values. In accordance with integrated enstrophy in Figure 11, $Fr = 0.5$ is the critical Fr number beyond which a further reduction of Fr increases the vortex stretching term. $Fr = 0.125$ and $Fr = 0.05$ wakes experience a higher peak in stretching by turbulent strain compared to the unstratified case. This increase is also observed in the stretching by the mean strain where $S2$ increases when $Fr < 0.5$. Reactivated velocity fluctuations and high velocity gradient in the vertical direction (the mean flow is reorganized into multiple two-dimensional layers) combine to increase $S2$. It is interesting to note that, while integrated enstrophy and their components shown in Figures 11 and 12 for $Fr = 0.25$ and 0.125 are larger than that of unstratified wake until the far end of the downstream domain, vortex stretching remains large only closer to the sphere and become less than unstratified stretching by $x/D \approx 3$. Regardless of the numerical approach one uses (LES, RANS) away from the body, it is thus imperative that the model accounts for motions near the sphere in these low-Fr wakes to capture the near-sphere enhancement of enstrophy that then lasts far downstream.

The stratified cases with $Fr \leq 0.125$ experience stronger vortex stretching compared with the unstratified case and stratified case at $Fr \geq 0.25$. The peaks of vortex stretching lie in the vicinity of highly rotational coherent vortices which shift upstream in the low Fr cases. Thus, as stratification increases, enstrophy is produced via a stretching mechanism closer to the sphere. Even with relatively high mean strain in the near wake compared to late wake, fluctuating strain still exceeds

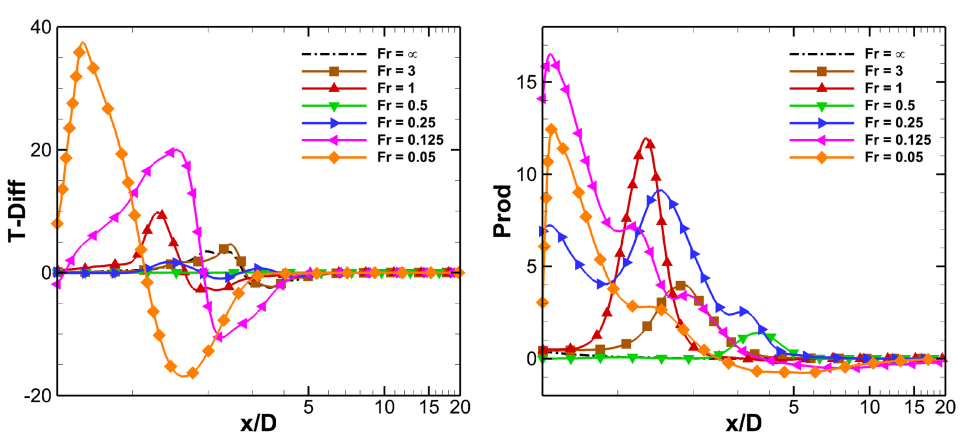

FIG. 16. Cross-sectional integration of turbulent diffusion (left) and production (right).

RIGHTSLINK

the mean strain resulting in the higher value of $S1$ compared to $S2$ in all cases.

While stretching and tilting by mean and fluctuating strain act mainly as the source, advection and dissipation balance them by being a transport and a sink of the enstrophy. Similar to the unstratified case, small scale dissipation remains the primary sink in the fluctuating enstrophy equation while mean advection acts secondarily. Unlike advection by mean flow, turbulent transport and production increase enstrophy near the sphere and decrease enstrophy further downstream as shown in Figure 16. Both transport and production terms are larger in magnitude in the low-Fr regime. Stretching, $S3$, and viscous diffusion term, $VDiff$ (not shown here) are two orders of magnitude smaller than $S1$ and do not significantly alter the enstrophy field.

V. SUMMARY AND CONCLUSIONS

DNS of flow past a sphere at Re = 3700 has been carried out in moderate-to-highly stratified cases and results with eight stratification levels of Fr = ∞, 3, 1, 0.5, 0.25, 0.125, 0.05, and 0.025 are reported; here, the unstratified case corresponds to $Fr = \infty$. Vortex dynamics is investigated by means of visualization of instantaneous vortical structures with the Q criterion, spatial distribution, and magnitude of enstrophy ($\overline{\omega_i'\omega_i'}$), and computation of terms in the enstrophy transport equation.

The Q criterion enables three-dimensional visualization of vortical structures. In the unstratified case, circular vortex rings are shed from the sphere which then break down into small structures after approximately one and a half times the sphere diameter. These small structures in the unstratified case are tube-like and show no preference in their orientation. Highly rotational vortex tubes are seen in the $1.5 < x/D < 5$ region behind the sphere and their rotational strength gradually decreases downstream. Moderate stratification, $Fr = O(1)$, preferentially orients vortex tubes in the streamwise direction but does not change their tube-like shape. At $0.25 < Fr < 1$, the lee wave impresses its undulation on the vortical structures.

High stratification, $Fr \leq 0.125$, significantly changes both the shape and orientation of the vortical structures. The cross section of vortex tubes is no longer circular but flattened. The orientation of the vortex tubes lies in the horizontal plane. At $Fr = 0.025$, isosurface of Q shows distinct pancake eddies and inclined surfboard structures, both structures being thin in the vertical. The pancake eddies are disc-like structures located in the central horizontal plane that occur alternately on each side with an offset from the center line and have an alternating sign of vertical vorticity. The surfboard structures are located in the middle, are inclined with the horizontal, and form successive V-shaped structures. The pancakes are regularly spaced with distance between two consecutive pancake eddies on the same side approximately $5D$ corresponding to the energy spectrum peak at Strouhal number of 0.2 associated with vortex shedding. Surfboard structures are shed with the same frequency as the pancake eddies. Thus, pancake eddies that occur in the near wake when the stratification is high are associated with the dominant vortex shedding mode at $Re = 3700$. The vorticity pattern is akin to that of a sinuous mode. The behavior at higher Re or at moderate-to-low stratification ($Fr \geq O(1)$) requires further exploration.

The distribution of enstrophy ($\overline{\omega_i'\omega_i'}$) across the wake cross section is isotropic in the unstratified case. Stratification distorts this distribution from circular to elliptical, close to the sphere. The enstrophy magnitude decreases with increasing stratification until Fr of 0.5. In contrast, there is a rapid increase of enstrophy with increasing stratification when Fr is decreased to 0.125 and beyond. At $Fr = 0.25$, three distinct horizontal layers are found where relatively low enstrophy is sandwiched between the upper and lower layers with high enstrophy. With increasing stratification, these three layers are vertically located closer to each other leaving a small thin layer in the middle.

The enstrophy equation shows that the dominant balance in the unstratified wake is between vortex stretching and dissipation with secondary contributions from advection and turbulent diffusion. In the stratified wake, the dominant balance remains between vortex stretching and dissipation with the contribution of the baroclinic term being secondary. Thus, the implicit stratification effect on vortex stretching is responsible for the changes in enstrophy with stratification observed in the simulations. In particular, stratified wakes with $Fr < 0.125$ have large vortex stretching in the region near the body that is associated with unsteady and intermittent shedding of the boundary layer from various vertical locations at the sides of the sphere. The vortex stretching in the region $x/D < 2$ is sufficiently large so that the enstrophy remains larger than in the unstratified case far downstream. The implication is that it is important to resolve the near-body flow for low-Fr wakes in order to obtain accurate results for the far wake. Simulations will have to be continued into the quasi–2D regime for $Fr \geq O(1)$ to investigate the persistence of near-body flow characteristics.

ACKNOWLEDGMENTS

I (Sutanu Sarkar) am pleased to contribute this paper in honor of John Lumley, who taught me turbulence and, more importantly, how to do research. John Lumley introduced me to the importance of vortex stretching in turbulence dynamics and the enstrophy equation. This paper considers vortex dynamics in stratified flows through structure education, enstrophy statistics, and the enstrophy equation. It is gratifying to acknowledge John Lumley's training that enabled me to do this work with my students Karu Chongsiripinyo and Anikesh Pal. We gratefully acknowledge the support of ONR Grant No. N00014-15-1-2718, program manager Tom Fu.

[1] J. T. Lin and Y. H. Pao, "Wakes in stratified fluids," Annu. Rev. Fluid Mech. **11**, 317–338 (1979).
[2] H. Hanazaki, "A numerical study of three-dimensional stratified flow past a sphere," J. Fluid Mech. **192**, 393–419 (1988).
[3] J. M. Chomaz, P. Bonneton, A. Butet, M. Perrier, and E. J. Hopfinger, "Froude number dependence of the flow separation line on a sphere towed in a stratified fluid," Phys. Fluids **4**(2), 254–258 (1992).
[4] J. M. Chomaz, P. Bonneton, and E. J. Hopfinger, "The structure of the near wake of a sphere moving horizontally in a stratified fluid," J. Fluid Mech. **254**, 1–21 (1993).

RIGHTSLINK

[5]G. R. Spedding, "The evolution of initially turbulent bluff-body wakes at high internal Froude number," J. Fluid Mech. **337**, 283–301 (1997).
[6]H. P. Pao and T. W. Kao, "Vortex structure in the wake of a sphere," Phys. Fluids **20**(2), 187–191 (1977).
[7]G. R. Spedding, "Anisotropy in turbulence profiles of stratified wakes," Phys. Fluids **13**(8), 2361–2372 (2001).
[8]M. Bonnier, P. Bonneton, and O. Eiff, "Far-wake of a sphere in a stably stratified fluid: Characterization of the vortex structures," Appl. Sci. Res. **59**(2-3), 269–281 (1998).
[9]M. J. Gourlay, S. C. Arendth, D. C. Fritts, and J. Werne, "Numerical modeling of initially turbulent wakes with net momentum," Phys. Fluids **13**(12), 3783–3802 (2001).
[10]D. G. Dommermuth, J. W. Rottman, G. E. Innis, and E. A. Novikov, "Numerical simulation of the wake of a towed sphere in a weakly stratified fluid," J. Fluid Mech. **473**, 83–101 (2002).
[11]K. A. Brucker and S. Sarkar, "A comparative study of self-propelled and towed wakes in a stratified fluid," J. Fluid Mech. **652**, 373–404 (2010).
[12]P. J. Diamessis, G. R. Spedding, and J. A. Domaradzki, "Similarity scaling and vorticity structure in high Reynolds number stably stratified turbulent wakes," J. Fluid Mech. **671**, 52–95 (2011).
[13]R. Pasquetti, "Temporal/spatial simulation of the stratified far wake of a sphere," Comput. Fluids **40**(1), 179–187 (2011).
[14]G. Yun, D. Kim, and H. Choi, "Vortical structures behind a sphere at subcritical Reynolds numbers," Phys. Fluids **18**(1), 5102 (2006).
[15]G. Constantinescu and K. Squires, "Numerical investigation of flow over a sphere in the subcritical and supercritical regimes," Phys. Fluids **16**(5), 1449–1466 (2004).
[16]J. Jeong and F. Hussain, "On the identification of a vortex," J. Fluid Mech. **285**, 69–94 (1995).
[17]G. R. Spedding, "Vertical structure in stratified wakes with high initial Froude number," J. Fluid Mech. **454**, 71–112 (2002).
[18]A. Pal, S. Sarkar, A. Posa, and E. Balaras, "Regeneration of turbulent fluctuations in low-Froude number flow over a sphere at Reynolds number of 3700," J. Fluid Mech. **804**(R2), 1–11 (2016).
[19]J. Yang and E. Balaras, "An embedded-boundary formulation for large-eddy simulation of turbulent flows interacting with moving boundaries," J. Comput. Phys. **215**, 12–40 (2006).
[20]E. Balaras, "Modeling complex boundaries using an external force field on fixed cartesian grids in large-eddy simulations," Comput. Fluids **33**, 375–404 (2004).
[21]I. Rodriguez, R. Borell, O. Lehmkuhl, C. D. Perez Segarra, and A. Oliva, "Direct numerical simulation of the flow over a sphere at Re = 3700," J. Fluid Mech. **679**, 263–287 (2011).
[22]M. B. de Stadler, S. Sarkar, and K. A. Brucker, "Effect of the Prandtl number on a stratified turbulent wake," Phys. Fluids **22**(9), 095102 (2010).
[23]J. C. R. Hunt, A. A. Wray, and P. Moin, "Eddies, streams, and convergence zones in turbulent flows," Technical Report, CTR, 1988.
[24]H. Schlichting and K. Gersten, *Boundary Layer Theory* (Springer, 1968).
[25]H. J. Kim and P. A. Durbin, "Observations of the frequencies in a sphere wake and of drag increase by acoustic excitation," Phys. Fluids **31**, 3260–3265 (1988).
[26]H. Sakamoto and H. Haniu, "A study on vortex shedding from spheres in uniform flow," J. Fluid Eng. **112**, 386–392 (1990).
[27]V. Seidl, S. Muzaferija, and M. Perić, "Parallel DNS with local grid refinement," Appl. Sci. Res. **59**(4), 379–394 (1997).
[28]A. G. Tomboulides and S. A. Orszag, "Numerical investigation of transitional and weak turbulent flow past a sphere," J. Fluid Mech. **416**, 45–73 (2000).
[29]P. Parnaudeau, J. Carlier, D. Heitz, and E. Lamballais, "Experimental and numerical studies of the flow over a circular cylinder at Reynolds number 3900," Phys. Fluids **20**(8), 085101 (2008).
[30]H. Tennekes and J. L. Lumley, *A First Course in Turbulence* (The MIT Press, Cambridge, Massachusetts, 1972).

RIGHTSLINK